Experimental strategies to fabricate mechanically exfoliated graphene sub-nanofluidic devices

Kang, X.; Fu, W.; Schneider, F.G.

Carbon 234 (2025) 120005

Contents lists available at ScienceDirect

Carbon

journal homepage: www.elsevier.com/locate/carbon

Experimental strategies to fabricate mechanically exfoliated graphene sub-nanofluidic devices

Xiaofang Kang [a,b], Wangyang Fu [b,**], Grégory F. Schneider [a,*]

[a] Leiden Institute of Chemistry, Leiden University, Einsteinweg 55, 2333CC Leiden, the Netherlands
[b] Key Laboratory of Advanced Materials of Ministry of Education, School of Materials Science and Engineering, Tsinghua University, Shaw Technical Science Building, Beijing Haidian District, 100084, People's Republic of China

ARTICLE INFO

Keywords:
: graphene
ion transport
Nanopore
Transmembrane electrode
Delamination
Mechanical exfoliation

ABSTRACT

Mechanically exfoliated graphene is highly attractive for ion transport devices and transmembrane applications because of its crystallinity and minimum defects. However, the small size and difficulty in manipulating exfoliated graphene pose significant challenges in fabricating quantities of reliable devices to build statistically robust datasets. Here, we systematically investigate the experimental procedures involved in preparing free-standing graphene sub-nanofluidic devices, identifying potential pitfalls at each fabrication stage that may lead to chip damage, graphene delamination, leakage, and partial wetting. We propose potential solutions to overcome these challenges associated with the use of mechanically exfoliated graphene in device fabrication, aiming to facilitate the development of high-quality graphene-based devices, paving the way for more comprehensive experimental analysis of the transmembrane ion transport properties of graphene, enabling the advancement of two-dimensional materials in membranes applications.

1. Introduction

Graphene, a one-atom-thin material with a π-system and exceptional mechanical strength, has opened up many opportunities for various applications [1–3]. One promising application is its use as a barrier membrane for gas or ion separation. Research has demonstrated that graphene is impermeable to gases as small as He [4], so pristine graphene cannot achieve gas molecule sieving unless defects are introduced. In 2014, a study experimentally revealed that the smallest particle, a proton, can pass through the perfect single-layer graphene [5], opening up the possibility of using pristine graphene for proton separation. Recent studies have clarified that proton permeation primarily arises from nanoripples and wrinkles on the graphene surface, which stretch lattice strain in the graphene and reduce the barrier energy for protons [6]. However, the graphene used in this experiment was supported by a Nafion film rather than being fully suspended. The presence of Nafion may introduce doping effects or alter the hydrophobicity of the graphene surface, potentially influencing the mechanism of proton permeation. To fully understand this mechanism with pristine graphene, it is necessary to eliminate the influence of the Nafion support.

However, using free-standing graphene in sub-nanofluidic devices still faces challenges [7,8], such as the difficulty and time-consuming process of transferring micrometer-scale, perfect mechanically exfoliated graphene flakes [9,10] over the target area. These low fabrication success rates hinder large-scale production, limits statistically significant data acquisition, and therefore impair the device success rate preventing to further study ion transport phenomena.

To address these challenges and understand the factors hindering the practical application of graphene in sub-nanofluidic devices, we conducted a systematic investigation of the entire experimental workflow, from device preparation to final measurement. Our analysis pinpointed three critical factors behind the low device yield: (1) mechanical strain induced on the suspended graphene membrane during chip assembly (52.4 %), often resulting in complete delamination or damage. (2) Inadequate wetting and contamination issues (24.2 %), and (3) partial delamination of the graphene membrane (18.4 %). These factors collectively account for 95 % of the devices, highlighting their significance in the fabrication process and the need for targeted solutions to improve overall yield. We propose strategies to increase the success rate: (1) redesigning the flow cell with softer O-rings and enlarged central apertures to decrease the mechanical stress induced to the graphene

* Corresponding author.
** Corresponding author.
E-mail addresses: fwy2018@mail.tsinghua.edu.cn (W. Fu), g.f.schneider@chem.leidenuniv.nl (G.F. Schneider).

https://doi.org/10.1016/j.carbon.2025.120005
Received 8 October 2024; Received in revised form 8 January 2025; Accepted 10 January 2025
Available online 17 January 2025

membrane, (2) optimizing the hydrophilicity of clean transfer processes and implementing oxygen plasma treatment of the flow cell microchannels, and (3) integrating a robust adhesion layer to prevent delamination [11]. Understanding and improving the reliability and reproducibility of these devices, would shed light on the ion transport mechanisms and accelerate the development of potential applications such as proton-conducting membranes [5,6], water purification [12,13], ion sieving [14–17], and osmotic power generation devices [18,19].

2. Materials and methods

Natural graphite used for exfoliated graphene was obtained commercially from NGS Naturgraphit. All chemicals were purchased from Sigma-Aldrich and were used as received without further purification.

Oxygen plasma was generated using a capacitively coupled plasma system (Femto, Diener Electronic) at 40 kHz and 200 W at room temperature. To render the surface hydrophilic, a 200 W oxygen plasma treatment was applied for 10 seconds. Optical images were obtained with a Leica DM 2700 M Brightfield microscope containing a Leica MC 120 HD camera. Raman spectra were acquired using a WITEC alpha500 R Confocal Raman Imaging system with a 532 nm, 2 mW laser. Scanning electron microscopy (SEM) was performed using a JEOL SEM 6400 to assess the graphene coverage and identify damaged areas in devices that were leaking. SEM imaging was done under a high vacuum with a 10 kV accelerating voltage, 0.1 nA current, and ~10 mm working distance to the lense. Ionic transport measurements were conducted with an Axopatch 200B amplifier and a Digitizer 1550 (Molecular Devices), referenced to a saturated Ag/AgCl electrode, at room temperature within a Faraday cage on a vibration isolation table to minimize noise.

3. Result and discussion

We used the "Scotch tape" technique to isolate the single-layer graphene (Fig. S1) from graphite on a silicon wafer with a 285 nm-thick layer of silicon dioxide (SiO_2) [20]. Firstly, we identified monolayer graphene based on its optical contrast under the microscope [21,22]. Raman spectroscopy was then employed to distinguish between single-layer and multilayer graphene flake [23], with monolayer graphene identified by a sharp 2D peak (~2700 cm^{-1}), and a 2D peak intensity approximately four times higher than that of the G peak (~1580 cm^{-1}) intensity [24,25].

We transferred monolayer exfoliated graphene onto a silicon nitride (SiN) carried chip with a 1 μm-sized hole using the "wedging transfer" technique [26]. This method involves dropping a CAB polymer solution (30 mg/mL, cellulose acetate butyrate, i.e., CAB in ethyl acetate) onto the monolayer graphene flake area on a Si wafer to act as a protective mask, followed by a 10-minute solvent evaporation. The wafer is then treated with oxygen plasma to make its surface hydrophilic. Next, the freshly-treated wafer is dipped into the CAB solution and dry 10 minutes. The hydrophilic wafer with hydrophobic CAB polymer is submerged in water and wedged off the wafer by sliding it at an angle, causing the CAB film with monolayer graphene to peel off the Si wafer and float on the water's surface. Under a microscope, the monolayer graphene is precisely aligned with the target micropore on the SiN chip, which is submerged at the bottom of the water. By gradually removing the water between the graphene and the chip, we positioned the graphene over the ~1 μm hole. Finally, the CAB film is dissolved using ethyl

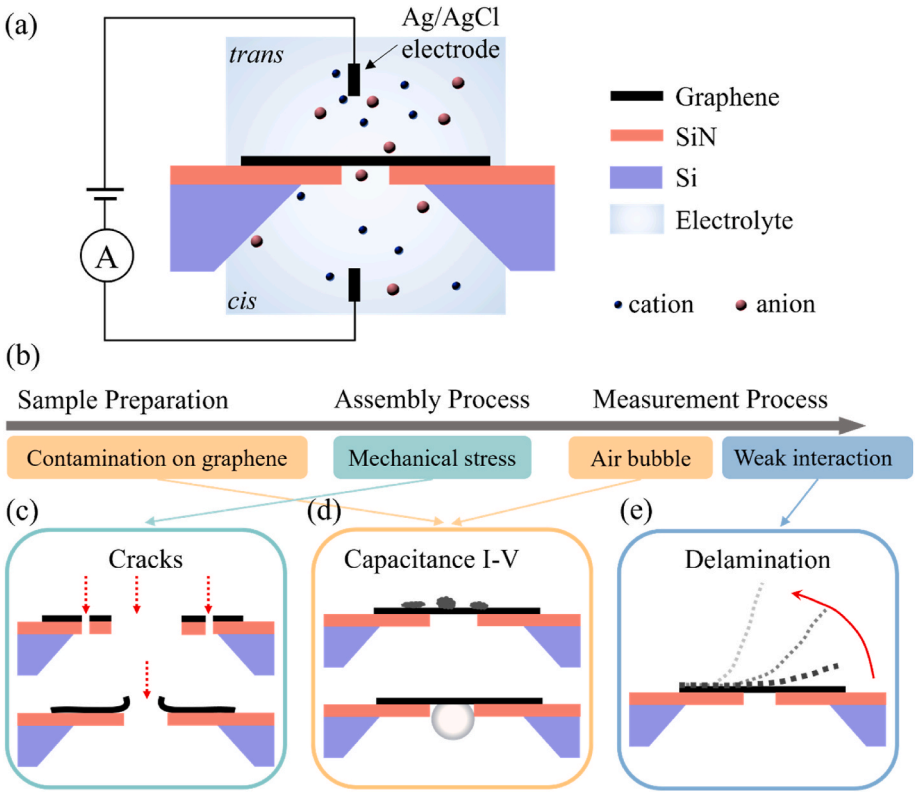

Fig. 1. Experimental setup and potential factors causing device breakdown in mechanically exfoliated graphene sub-nanofluidic devices. (a) Schematic of the measurement set-up, featuring a graphene membrane suspended over a micropore in a SiN chip, mounted in a microfluidic flow cell with cis and trans chambers. Ag/AgCl electrodes are used to apply a voltage and measure the ionic current. (b) Overview of the possible causes yielding to unsuccessful devices during sample preparation, assembly process, and measurement process. (c) Illustration of potential damage to the graphene or SiN membrane during the process of mounting the chip in the flow cell, which can lead to unintended current pathways. (d) Representative I–V curves showing capacitive behaviors, possibly caused by air bubbles due to graphene hydrophobicity or polymer residues from the transfer process. (e) Schematic of graphene delamination over time, resulting in increased leakage currents. (A colour version of this figure can be viewed online.)

acetate.

We mounted the graphene-on-chip into a microfluidic flow cell with two chambers, known as the "trans" and "cis". To wet the microflow channel, we injected a 1:1 (vol/vol) mixture of ethanol and ultrapure water into the inlets [27], followed by the injection of the electrolyte (0.1 M HCl) and the placement of Ag/AgCl electrodes. By applying a voltage across these two electrodes, we were able to measure an ion current (see Fig. 1a).

Our priority was to evaluate whether the assembly process (Fig. 1b) could potentially damage the graphene or the suspended SiN membrane (see Fig. 1c). Any damage to these membranes could create additional ionic current pathways, leading to leakage. If the graphene membrane remained intact after mounting the chip on the flow cell, we verified that ions transported only through the suspended graphene region as expected, rather than leaking through the interfacial channel between the graphene and the substrate. Also, over time, if graphene delaminated from the chips, we would expect to measure an increase in ion current due to uncontrolled leakage (Fig. 1e).

In addition to different causes of leakage, it is crucial to determine whether the measured conductance originates from the graphene itself or if other factors influenced the results. Also, non-linearities in conductance-voltage plots suggest the absence of an ion path: ions accumulate at the graphene-water interface intrinsically building up a capacitor. Moreover, very low conductances or non-linearities could be influenced by other factors such as air bubbles trapped in the pore, graphene hydrophobicity, or polymer residues introduced during the graphene transfer process (see Fig. 1d).

We first examine the critical process of mounting the chip in the flow cell. Our custom-designed polymethyl methacrylate (PMMA) flow cell comprises two separate parts, each featuring inlet and outlet ports for fluid flow. During assembly, we carefully sandwich the graphene-covered chip between these two parts, ensuring that the free-standing graphene areas align precisely with the inlet microchannels. To prevent liquid leakage, we securely affix O-rings to both sides of the chip and each part of the flow cell (Fig. S2). Following chip installation, we introduce 0.1 M HCl electrolyte through the inlet ports and place the Ag/AgCl electrodes in the inlet channels of each flow cell component to apply a direct current voltage across the graphene membrane. To avoid the risk of voltage-induced graphene breakdown [28], we used a small voltage range of −100 mV–100 mV, with 10 mV increments.

We tested a total of 103 devices with mechanically exfoliated graphene. Of these, 54 devices (52.4 %) exhibited conductivity equal to or exceeding that of bare chips with 1 μm pores. Conductivity equal to that of 1 μm holes indicates complete graphene removal, while higher conductivity suggests the presence of additional pathways beyond the pore itself. Post-measurement scanning electron microscopy (SEM) analysis revealed varying degrees of SiN membrane damage (Fig. 2a): (i) minor cracking of the SiN window with intact free-standing graphene, (ii) extensive SiN membrane damage, with pore area that is supposed to be covered by graphene, but no graphene anymore, and (iii) near-complete destruction of the SiN window.

The severity of this damage is particularly noteworthy given that both SiN and graphene membranes were intact before flow cell mounting. The results of significant leakage currents and extensive damage under SEM after loading implicate the loading process as the primary cause of membrane damage. That could be due to the force during chip installation to ensure a tight seal with the O-rings, which are critical for eliminating gaps between flow cell components and chips.

We found that the nitrile compound O-rings used in our flow cell with high hardness and poor viscoelasticity, resulting in a limited contact area with the chip (Fig. 2b and c). This limited contact area hindered the O-ring's ability to conform to the chip surface, leading to localized stress concentrations at the membrane interface. During the mounting process, the rigid O-ring material likely exerted excessive mechanical stress on the membrane, potentially inducing cracks or breaks (Fig. 2d). Our analysis revealed that the majority of unsuccess can be traced to mechanical stresses induced by measurement setups (flow cells) during the device assembly process. Notably, 49 devices (47.6 %) did not show such a high leakage, due to cautious operation during the chip mounting step.

After excluding devices with high leakage, we encountered a subset of samples exhibiting extreme I–V curve asymmetry, indicative of capacitive rather than resistive characteristics. We categorized these samples into three groups: (1) Ultra-low conductance (8 out of the 103 devices, 7.8 %): these devices exhibited a low 10 pA current (Fig. 3a), suggesting near-complete blockage within the pore region. We hypothesize that this phenomenon may be attributed to the presence of nanobubbles [29], either on the graphene surface or on microflow channels's walls, impeding ion transport (Fig. 3d). (2) Subtle asymmetry (9 devices, 8.7 %): These samples displayed mild asymmetry under an applied voltage of −100 mV (Fig. 3b). (3) High-current asymmetry (8 devices, 7.8 %): this group exhibited elevated currents coupled with pronounced

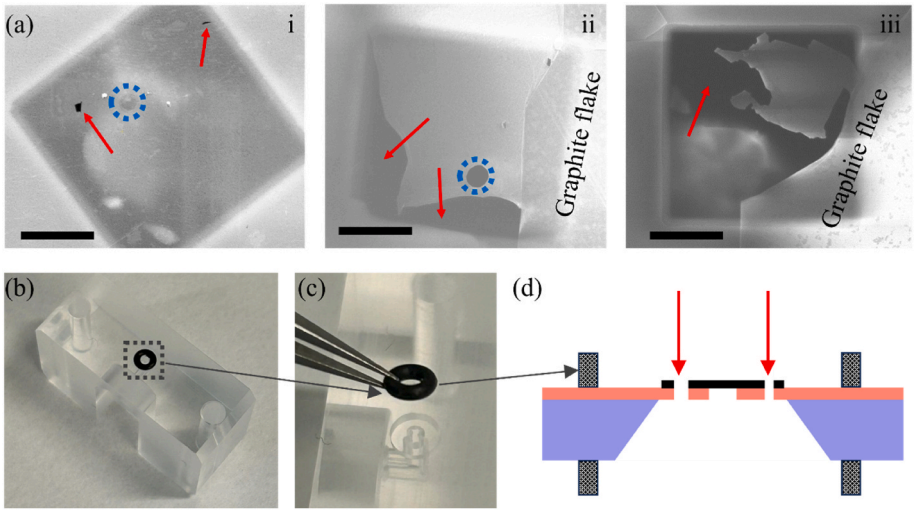

Fig. 2. Analysis of device breakdown due to strain caused by an inadequate flow cell design. (a) SEM images revealing damage to the SiN window after ionic transport measurements: (i) localized crack (red arrow) with intact free-standing graphene (blue dashed circle), (ii) Extensive damage to the SiN membrane and loss of free-standing graphene, (iii) Near-complete rupture of the SiN membrane. Scale bar: 4 μm. (b,c) Photographs of the custom-designed flow cell, highlighting the O-ring component. (d) Schematic cross-section illustrating the process of the chip loading with the O-ring, showing localized pressure distribution and potential crack formation sites. (For interpretation of the references to colour in this figure legend, the reader is referred to the Web version of this article.)

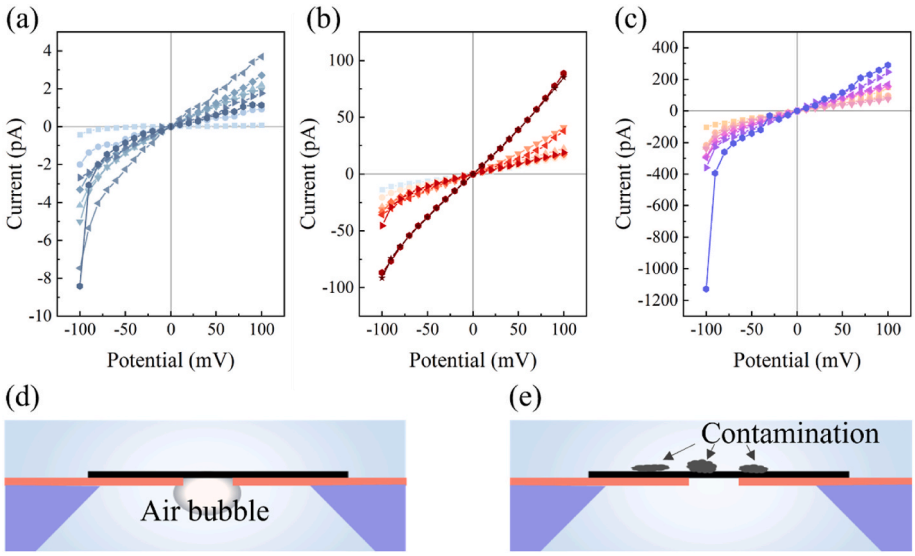

Fig. 3. Asymmetric I–V curves and underlying mechanisms. (a) Ultra-low current regime, (b) subtle asymmetry in low current regime, and (c) asymmetry coupled with large currents. (d) Schematic illustration of nanobubble-induced ion transport obstruction, corresponding to the ultra-low conductance regime in (a). (e) Conceptual model of non-uniform surface charge distribution caused by contaminants, leading to asymmetric I–V characteristics observed in (b) and (c). (A colour version of this figure can be viewed online.)

asymmetry (Fig. 3c).

The asymmetry observed in Fig. 3b and c can be induced by various factors, such as the geometry of channel, and also a non-uniform surface charge distribution [30]. However, in our experiments we only used monolayer graphene, eliminating inherent asymmetry in the channel geometry. Instead, we propose that this asymmetry stems from non-uniform charge distribution along the graphene channel, likely caused by residual polymer from the transfer process or adsorbed airborne contaminants on the graphene surface (Fig. 3e). These factors can induce localized charge, resulting in the observed asymmetric I–V curves. In total, 24 devices (24.2 % of the 103 devices) exhibited this asymmetric behavior and were consequently excluded from further analysis.

Analysis of the remaining 24 devices revealed two subsets with

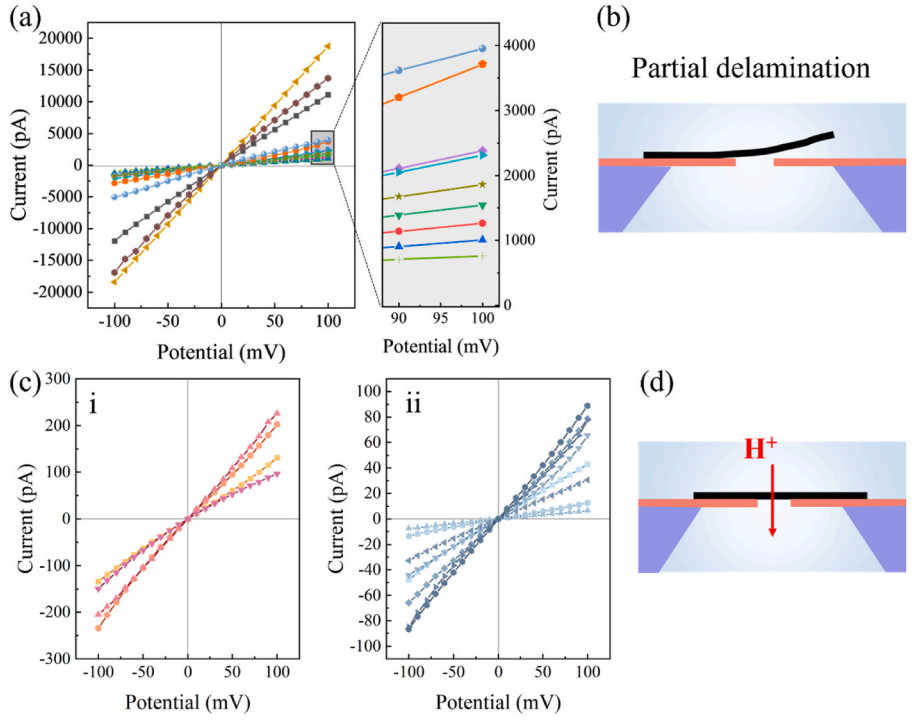

Fig. 4. Symmetric and linear I–V curves for partially delaminated devices and non-delaminated devices. (a) I–V curves of 12 devices (11.7 %) exhibiting partial delamination, with currents ranging from 1 nA to 20 nA at 100 mV. Inset: Magnified view of the 90–100 mV range for nine representative devices. (b) Schematic cross-section illustrating partial graphene delamination, explaining the mechanism for high conductance observed in (a). (c) I–V curves of devices displaying expected graphene behavior: (i) four devices with areal conductances of 0.17, 0.30, 0.26, and 0.19 S cm^{-2}, and (ii) eight devices exhibiting lower areal conductances ranging from 0.01 to 0.1 S cm^{-2}. (d) Conceptual model of selective proton transport through an intact graphene membrane in a nanofluidic device. (A colour version of this figure can be viewed online.)

different conductances. The first subset, comprising 12 devices (11.7 % of the total), exhibited I–V curves with currents ranging from 1 nA to 20 nA at 100 mV (Fig. 4a). These devices displayed areal conductance values between 1 and 25 S cm^{-2}, significantly exceeding previously reported proton conductance values for graphene [31]. We attribute this anomalously high conductance to partial delamination of the graphene membrane from the substrate (Fig. 4b), resulting in the formation of additional ionic current pathways.

The second subset, also comprising 12 devices (11.7 % of the total), demonstrated linear I–V curves and low conductance values when measured in 0.1 M HCl solution. This linearity precludes graphene surface contamination and charge-induced I–V asymmetry as potential factors. The observed low conductance aligns with values reported in the literature [31], suggesting minimal contribution from leakage currents and a dominant role of the intrinsic properties of the graphene membrane in determining its conductance (Fig. 4d). Four of these 12 devices displayed currents ranging from 100 pA to 250 pA at 100 mV (Fig. 4c(i)), corresponding to areal conductances spanning from 0.17 to 0.30 S cm^{-2}. The remaining eight devices demonstrated lower areal conductances, ranging from 0.01 to 0.1 S cm^{-2} (Fig. 4c(ii)). The conductivity values for a subset of these devices vary by less than an order of magnitude, indicating consistent and reproducible graphene properties. This final group of 12 devices, representing 11.7 % of the total number of samples, most closely reflects the expected behavior of pristine graphene membranes. The observed conductance in these devices likely includes contributions from nanoripples and wrinkles on the graphene surface, which are unavoidably introduced during the graphene transfer process. These morphologies create localized curvature and strain in graphene lattice, which were reported to lower the proton energy barrier, facilitate proton adsorption, and create preferential pathways for proton transport [6].

To further study the long-term stability of the 12 successful devices, we tested the graphene transconductance in various electrolyte solutions (0.1 M of HCl, KCl, $CuCl_2$, $CaCl_2$, $FeCl_3$) by repeatedly exchanging the electrolyte. Seven devices showed increased conductance, eventually matching that of the chip itself (Fig. 5a) after multiple exchange cycles. From the images captured before performing I-V measurements, monolayer graphene can be seen over the 1 μm pore area, with surrounding graphite flakes serving as a reference (we can also see this from Fig. 2a(ii) and (iii)). However, after-ion transport measurement, the graphene flake was gone from the chip (Fig. 5c). This delamination can be attributed to the small size of mechanically exfoliated graphene flakes (~10 μm in diameter). Although monolayer graphene initially covered the hole, the exposed edges and hydrophilicity of the silicon nitride surface increase the probability for water to intercalate from the edge area of the graphene flake to in between the flake and the substrate, leading to gradual delamination (Fig. 5b).

Our findings, based on statistical analyses of the 103 device situations (as summarized in Table S1), highlight the need to reduce mechanical strain, reduce contamination, increase wetting, and avoid delamination through innovative design solutions and optimized fabrication protocols. We propose some approaches to tackle these challenges. Firstly, to mitigate stress-induced graphene damage during the chip mounting, we propose optimizing the flow cell design. Specifically, we suggest fabricating a sample chamber with dimensions precisely tailored to the chip specifications, ensuring appropriate chamber height to minimize the loading process (Fig. S3). Additionally, incorporating softer O-rings with larger contact areas can evenly distribute residual stress evenly across the chip surface. Furthermore, increasing the central aperture size of the O-rings allows their position further from the suspended membrane (Fig. S4), reducing localized stress on the fragile membrane. Secondly, to minimize contaminant residues, we recommend implementing refined graphene transfer protocols, for example using cleaner polymers, such as paraffin instead of PMMA as reported by Kong et al. [32]. Additionally, by optimizing the removal of residues for example by controlled heating during the polymer removal step or post-transfer annealing, has further contributed to reducing contamination. Thirdly, to address poor wetting, we suggest to (1) treat the flow cell microchannels with oxygen plasma before loading the chip, rendering channel surfaces hydrophilic, and (2) improve the wetting by

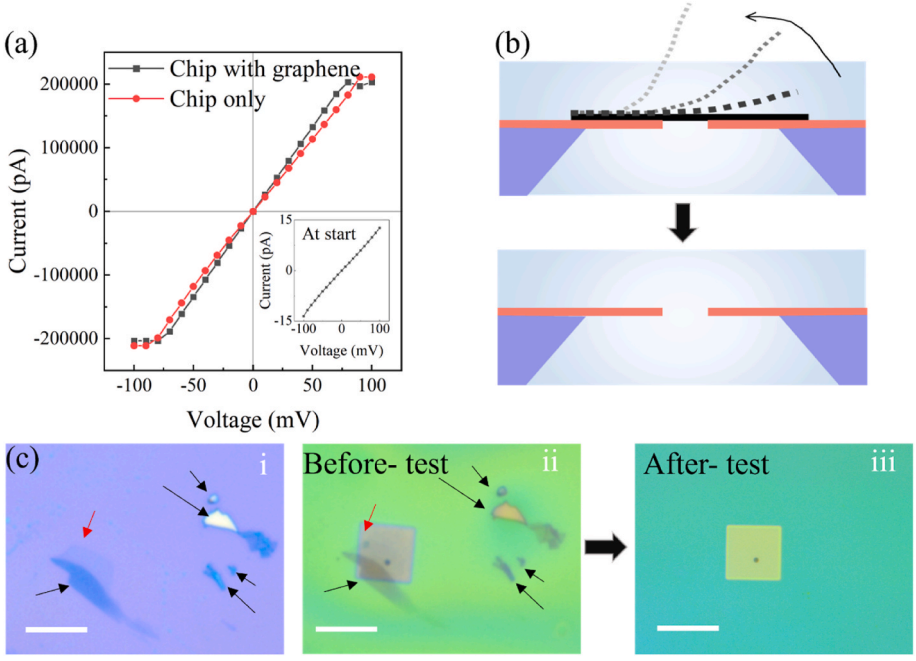

Fig. 5. Time-dependent delamination of graphene in nanofluidic devices: (a) I–V curves of seven devices (out of 12) exhibiting time-lapse graphene delamination. (b) Schematic of the gradual graphene delamination process. (c) Optical image: (i) mechanically exfoliated monolayer graphene (red arrow) and reference graphite flake (black arrow) on a silicon wafer. (ii) Chip with transferred graphene before testing. (iii) Post-test chip surface, showing the absence of both graphene layer and reference flakes, indicating complete delamination. Scale bar: 20 μm. (For interpretation of the references to colour in this figure legend, the reader is referred to the Web version of this article.)

using a 1:1 ethanol-water solution. Increasing the number of rinsing cycles and extending soaking time with this 1:1 ethanol-water solution could enhance the wetting of the chip wetting, ensuring also a better contact between the electrolyte and the graphene. Lastly, to prevent the gradual delamination of graphene, enhancing the adhesion energy between the membrane and substrate is important. We propose to pre-coating chips with hydrophobic self-assembled monolayers such as hexamethyldisilazane or octadecyltrichlorosilane. These coatings create a interfacial layerincreasing the interaction between the graphene and the substrate.

4. Conclusions

This study systematically investigated the fabrication process of mechanically exfoliated graphene sub-nanofluidic devices through comprehensive statistical analysis. Our examination revealed that devices break at different stages: 52.4 % of devices damaged during the mounting of the chip due to mechanical stress, 16.5 % were affected by contaminant residues during graphene transfer, 7.8 % exhibited poor wetting, and 11.7 % showed large leakage currents at the graphene-substrate interface. Notably, only 11.6 % of devices demonstrated intrinsic graphene transmembrane properties, with proton conductance ranging from 0.01 to 0.3 S cm^{-2}. However, 58.3 % of these experienced gradual delamination, resulting in a mere 4.9 % of devices remaining stable throughout testing.

These findings provide crucial insights into the challenges impeding successful device fabrication and guiding targeted solutions. We propose approaches to address these issues, including: (1) optimized flow cell designs to mitigate mechanical stress, (2) cleaner transfer protocols to minimize contamination, (3) enhanced wetting/sealing strategies, and (4) surface modifications to prevent delamination. This comprehensive understanding enables the fabrication of less-delaminating mechanically exfoliated graphene sub-nanofluidic systems, deepening insights into ion transport mechanisms, particularly proton, and facilitating their integration into applications like proton-conducting membranes, ionic/molecular sieving, biosensing, and energy harvesting.

CRediT authorship contribution statement

Xiaofang Kang: Writing – review & editing, Writing – original draft, Visualization, Validation, Investigation, Funding acquisition, Formal analysis, Data curation. **Wangyang Fu:** Writing – review & editing, Supervision, Methodology. **Grégory F. Schneider:** Writing – review & editing, Validation, Supervision, Software, Resources, Project administration, Methodology, Investigation, Funding acquisition.

Declaration of competing interest

The authors declare that they have no known competing financial interests or personal relationships that could have appeared to influence the work reported in this paper.

Acknowledgments

This research was supported by the European Research Council under the European Union's Seventh Framework Programme (FP/2007–2013)/ERC Grant Agreement no.335879 project acronym "Biographene" and the Netherlands Organization for Scientific Research (NWO) VIDI 723.013.007, awarded to G.F. Schneider. The authors acknowledge the financial support from the China Scholarship Council (No. 202107720043).

Appendix A. Supplementary data

Supplementary data related to this article can be found at https://doi.org/10.1016/j.carbon.2025.120005.

References

[1] K.S. Novoselov, A.K. Geim, S.V. Morozov, D. Jiang, Y. Zhang, S.V. Dubonos, et al., Electric field effect in atomically thin carbon films, Science 306 (5696) (2004) 666–669.
[2] A.K. Geim, K.S. Novoselov, The rise of graphene, Nat. Mater. 6 (3) (2007) 183–191.
[3] A.H. Castro Neto, F. Guinea, N.M.R. Peres, K.S. Novoselov, A.K. Geim, The electronic properties of graphene, Rev. Mod. Phys. 81 (1) (2009) 109–162.
[4] J.S. Bunch, S.S. Verbridge, J.S. Alden, A.M. van der Zande, J.M. Parpia, H. G. Craighead, P.L. McEuen, Impermeable atomic membranes from graphene sheets, Nano Lett. 8 (8) (2008) 2458–2462.
[5] S. Hu, M. Lozada-Hidalgo, F.C. Wang, A. Mishchenko, F. Schedin, R.R. Nair, et al., Proton transport through one-atom-thick crystals, Nature 516 (7530) (2014) 227–230.
[6] O.J. Wahab, E. Daviddi, B. Xin, P.Z. Sun, E. Griffin, A.W. Colburn, et al., Proton transport through nanoscale corrugations in two-dimensional crystals, Nature 620 (7975) (2023) 782–786.
[7] G.F. Schneider, S.W. Kowalczyk, V.E. Calado, G. Pandraud, H.W. Zandbergen, L. M. Vandersypen, C. Dekker, DNA translocation through graphene nanopores, Nano Lett. 10 (8) (2010) 3163–3167.
[8] C.A. Merchant, K. Healy, M. Wanunu, V. Ray, N. Peterman, J. Bartel, et al., DNA translocation through graphene nanopores, Nano Lett. 10 (8) (2010) 2915–2921.
[9] M. Lozada-Hidalgo, S. Zhang, S. Hu, V.G. Kravets, F.J. Rodriguez, A. Berdyugin, et al., Giant photoeffect in proton transport through graphene membranes, Nat. Nanotechnol. 13 (4) (2018) 300–303.
[10] E. Griffin, L. Mogg, G.P. Hao, G. Kalon, C. Bacaksiz, G. Lopez-Polin, et al., Proton and Li-ion permeation through graphene with eight-atom-ring defects, ACS Nano 14 (6) (2020) 7280–7286.
[11] B.S. Can, N.V.V. Blümel, E.P. van Geest, M. Makurat, J.M. van Ruitenbeek, G. F. Schneider, A Perspective on graphene junctions for recognition tunneling, Appl. Phys. Lett. 124 (21) (2024).
[12] M. Heiranian, A.B. Farimani, N.R. Aluru, Water desalination with a single-layer MoS2 nanopore, Nat. Commun. 6 (2015) 8616.
[13] S.P. Surwade, S.N. Smirnov, I.V. Vlassiouk, R.R. Unocic, G.M. Veith, S. Dai, S. M. Mahurin, Water desalination using nanoporous single-layer graphene, Nat. Nanotechnol. 10 (5) (2015) 459–464.
[14] J. Abraham, K.S. Vasu, C.D. Williams, K. Gopinadhan, Y. Su, C.T. Cherian, et al., Tunable sieving of ions using graphene oxide membranes, Nat. Nanotechnol. 12 (6) (2017) 546–550.
[15] Y. Qian, J. Shang, D. Liu, G. Yang, X. Wang, C. Chen, et al., Enhanced ion sieving of graphene oxide membranes via surface amine functionalization, J. Am. Chem. Soc. 143 (13) (2021) 5080–5090.
[16] L. Guo, Y. Liu, H. Zeng, S. Zhang, R. Song, J. Yang, et al., Covalently functionalized nanopores for highly selective separation of monovalent ions, Adv. Mater. 36 (1) (2024) e2307242.
[17] S. Yasuda, H. Matsushima, K. Harada, R. Tanii, T.O. Terasawa, M. Yano, et al., Efficient hydrogen isotope separation by tunneling effect using graphene-based heterogeneous electrocatalysts in electrochemical hydrogen isotope pumping, ACS Nano 16 (9) (2022) 14362–14369.
[18] X. Liu, M. He, D. Calvani, H. Qi, K. Gupta, H.J.M. de Groot, et al., Power generation by reverse electrodialysis in a single-layer nanoporous membrane made from core-rim polycyclic aromatic hydrocarbons, Nat. Nanotechnol. 15 (4) (2020) 307–312.
[19] J. Safaei, G. Wang, Progress and prospects of two-dimensional materials for membrane-based osmotic power generation, Nano Res. Energy 1 (2022).
[20] K.S. Novoselov, D. Jiang, F. Schedin, T.J. Booth, V.V. Khotkevich, S.V. Morozov, A. K. Geim, Two-dimensional atomic crystals, Proc. Natl. Acad. Sci. U. S. A. 102 (30) (2005) 10451–10453.
[21] P. Blake, E.W. Hill, A.H. Castro Neto, K.S. Novoselov, D. Jiang, R. Yang, et al., Making graphene visible, Appl. Phys. Lett. 91 (6) (2007).
[22] Z.H. Ni, H.M. Wang, J. Kasim, H.M. Fan, T. Yu, Y.H. Wu, et al., Graphene thickness determination using reflection and contrast spectroscopy, Nano Lett. 7 (9) (2007) 2758–2763.
[23] L.M. Malard, M.A. Pimenta, G. Dresselhaus, M.S. Dresselhaus, Raman spectroscopy in graphene, Phys. Rep. 473 (5–6) (2009) 51–87.
[24] A.C. Ferrari, J.C. Meyer, V. Scardaci, C. Casiraghi, M. Lazzeri, F. Mauri, et al., Raman spectrum of graphene and graphene layers, Phys. Rev. Lett. 97 (18) (2006) 187401.
[25] D. Graf, F. Molitor, K. Ensslin, C. Stampfer, A. Jungen, C. Hierold, L. Wirtz, Spatially resolved Raman spectroscopy of single- and few-layer graphene, Nano Lett. 7 (2) (2007) 238–242.
[26] G.F. Schneider, V.E. Calado, H. Zandbergen, L.M. Vandersypen, C. Dekker, Wedging transfer of nanostructures, Nano Lett. 10 (5) (2010) 1912–1916.
[27] M. Graf, M. Lihter, M. Thakur, V. Georgiou, J. Topolancik, B.R. Ilic, et al., Fabrication and practical applications of molybdenum disulfide nanopores, Nat. Protoc. 14 (4) (2019) 1130–1168.
[28] J. Loessberg-Zahl, D.S. de Bruijn, W.T.E. van den Beld, E. Dollekamp, E. Grady, A. Keerthi, et al., Exploring voltage mediated delamination of suspended 2D materials as a cause of commonly observed breakdown, J. Phys. Chem. C 124 (1) (2019) 430–435.
[29] E. Beamish, H. Kwok, V. Tabard-Cossa, M. Godin, Precise control of the size and noise of solid-state nanopores using high electric fields, Nanotechnology 23 (40) (2012) 405301.

[30] L.J. Cheng, L.J. Guo, Nanofluidic diodes, Chem. Soc. Rev. 39 (3) (2010) 923–938.
[31] S. Garaj, W. Hubbard, A. Reina, J. Kong, D. Branton, J.A. Golovchenko, Graphene as a subnanometre trans-electrode membrane, Nature 467 (7312) (2010) 190–193.
[32] W.S. Leong, H. Wang, J. Yeo, F.J. Martin-Martinez, A. Zubair, P.C. Shen, et al., Paraffin-enabled graphene transfer, Nat. Commun. 10 (1) (2019) 867.